

Cite this: *Catal. Sci. Technol.*, 2017,  
7, 4893

## Metal–organic frameworks (MOFs) for photocatalytic CO<sub>2</sub> reduction

Yi Chen, Dengke Wang, Xiaoyu Deng and Zhaohui Li \*

The utilization of solar energy for CO<sub>2</sub> conversion to produce valuable chemicals or fuels is extremely appealing since it can simultaneously reduce the greenhouse effect and relieve the energy shortage pressure. In addition to the commonly used semiconductor-based photocatalysts, metal–organic frameworks (MOFs), a class of micro-mesoporous hybrid materials, are recently emerging as new types of photoactive materials for CO<sub>2</sub> reduction due to their excellent adsorption capability toward CO<sub>2</sub> and unique structural characteristics. In this review, we summarized the recent applications of MOFs for photocatalytic CO<sub>2</sub> reduction, in which MOFs either act directly as the photocatalysts for CO<sub>2</sub> reduction or as components in a hybrid photocatalytic system to promote CO<sub>2</sub> reduction. This review starts with a brief introduction of the background of photocatalytic CO<sub>2</sub> reduction, followed by a summarization of CO<sub>2</sub> reduction catalyzed by photoactive ligands and metal nodes in MOFs, respectively. Thereafter, the construction of hybrid photocatalytic systems in which MOFs play a role in promoting photocatalytic CO<sub>2</sub> reduction is described. Finally, the limitations, challenges and future prospects of the application of MOFs to CO<sub>2</sub> reduction are addressed. We hope that this review not only can serve as a starting point to get into this largely unexplored field but can also stimulate intensive research on the rational design and development of more creative MOF systems for light induced CO<sub>2</sub> conversion, which is a green and sustainable strategy for CO<sub>2</sub> utilization.

Received 14th August 2017,  
Accepted 11th September 2017

DOI: 10.1039/c7cy01653k

rsc.li/catalysis

### 1. Introduction

Increased emission of carbon dioxide (CO<sub>2</sub>) from the combustion of fossil fuels is the primary cause of global warming. As compared with the currently adopted carbon capture and sequestration/separation approach, the utilization of CO<sub>2</sub> as a chemical feedstock for producing valuable chemicals/fuels to realize a carbon neutral cycle is a more desirable approach since it can simultaneously reduce the greenhouse effect and relieve the energy shortage pressure. In particular, the utilization of abundant solar energy for the conversion of CO<sub>2</sub> is extremely appealing. However, CO<sub>2</sub> is the most stable form of carbon, which makes its reduction to form chemicals very challenging. To date, extensive efforts have already been devoted to developing photocatalysts for CO<sub>2</sub> reduction and a number of excellent reviews in this field have already been reported.<sup>1</sup> The examined photocatalysts include semiconductors, homogeneous molecular complexes, metal-incorporated zeolites and metal–organic frameworks (MOFs). However, the performance for CO<sub>2</sub> reduction over the already investigated photocatalysts is still low. There is an urgent need to develop

highly efficient photocatalysts for converting CO<sub>2</sub> into useful chemicals.

MOFs are a class of 3D crystalline micro-/mesoporous hybrid materials constructed from metal or metal cluster nodes interconnected with multi-dentate organic linkers, which have already shown a variety of applications.<sup>2</sup> The modular nature of MOFs makes it feasible to develop MOF-based photocatalysts by immobilizing photoactive catalytic sites in MOFs. Both the metal nodes and the organic linkers in MOFs can be tailored for their use in photocatalysis.<sup>3</sup> It is generally accepted that the metal nodes can act as semiconductor QDs, while the organic linkers can act as the antenna to sensitize these QDs, based on the pioneering studies by Zecchina, García and Majima on MOF-5, a widely studied Zn-containing MOF material.<sup>4</sup> In addition, the organic ligands of MOFs can also be activated *via* photoactive metalloligands or dyes, either as building blocks to construct the MOFs, or grafted on the structure as a photoactive part on the organic ligand *via* a post-synthetic method.<sup>5</sup> The highly crystalline nature of MOFs ensures the charge transfer from the light-excited organic linker to metal clusters, while the existence of adjustable pores with different topology can facilitate the mass transport during the reaction, which makes the MOFs superior photocatalysts. In addition, the tailorable character of MOFs provided by the availability of a large variety of organic ligands and the rich coordination chemistry of

Research Institute of Photocatalysis, State Key Laboratory of Photocatalysis on Energy and Environment, College of Chemistry, Fuzhou University, Fuzhou, 350116, P. R. China. E-mail: zhaohuili1969@yahoo.com

transition metal cations allow huge flexibility for the successful tuning of light absorption to realize efficient utilization of solar energy, which is unmatched by semiconductor-based photocatalysts. With all these advantages, MOFs have been successfully applied in a variety of photocatalytic reactions, including CO<sub>2</sub> reduction,<sup>6</sup> hydrogen evolution,<sup>7</sup> pollutant degradation<sup>8</sup> and organic transformations.<sup>9</sup> In particular, MOFs have great potential for photocatalytic CO<sub>2</sub> reduction, since MOFs have been extensively studied as adsorbents for CO<sub>2</sub><sup>10</sup> and heterogeneous catalysts for CO<sub>2</sub> chemical transformation<sup>11</sup> ascribed to their excellent adsorption capability toward CO<sub>2</sub> and the presence of a large number of catalytic sites. Therefore, the application of MOFs for photocatalytic CO<sub>2</sub> reduction has attracted considerable research interest in the past few years.

However, as compared with semiconductors and homogeneous molecular complexes, MOFs are relatively new as photocatalysts for CO<sub>2</sub> reduction and currently their great potential in this field remains largely unexploited. Several excellent reviews on using MOFs in photocatalysis have already appeared, but none of them focus on photocatalytic CO<sub>2</sub> reduction.<sup>12</sup> Therefore, we believe that a comprehensive and up-to-date review summarizing the recent applications of MOFs for CO<sub>2</sub> reduction that have appeared at this time not only can serve as a starting point to get into this largely unexplored field but can also stimulate intensive research on the rational design and development of more creative MOF systems for light induced CO<sub>2</sub> conversion, which is a green and sustainable strategy for CO<sub>2</sub> utilization. This review starts with a brief introduction of the background of photocatalytic CO<sub>2</sub> reduction. The second and third parts summarize the use of MOFs as photocatalysts for CO<sub>2</sub> reduction, in which photoactive ligands and photoactive metal nodes are involved, respectively. The use of MOFs as cocatalysts to promote photocatalytic CO<sub>2</sub> reduction in a hybrid system is summarized in the fourth part. The limitations, challenges and future prospects of the application of MOFs for CO<sub>2</sub> reduction are addressed in the final section.

## 2. CO<sub>2</sub> reduction initiated by photoactive ligands in MOFs

Homogeneous metal complexes containing Ru, Re, Ir *etc.* as well as some porphyrin-based compounds have long been examined for photocatalytic CO<sub>2</sub> reduction.<sup>13</sup> Although tremendous progress has been made in the design and syntheses of homogeneous molecular complexes for CO<sub>2</sub> reduction in the past decades, and in some cases even the reaction efficiency can be comparable to that of photosystem II *in vivo*, generally homogeneous metal complexes lack long term stability.<sup>14</sup> In addition, homogeneous systems suffer from difficult separation from the reaction mixture, product contamination and limited recyclability of the catalysts. Therefore, it is desirable to develop analogous reusable heterogeneous photocatalysts for CO<sub>2</sub> reduction.

Due to their high surface areas and uniform but tailorable pores for facile diffusion of reactants, MOFs are suitable hosts or supports for homogeneous metal complexes. As compared to other solid supports which have non-homogeneously scattered sites, MOFs can be endowed with well-defined and isolated sites for the anchoring of the catalytic species, which makes them appealing for constructing supported single site catalysts.<sup>15</sup> The use of photoactive organo/metal-organo complexes as linkers to construct MOFs can produce photocatalytic active MOFs with isolated catalytic sites, which not only can maintain or even show improved performance as compared with their homogeneous counterparts but also show the advantage of being heterogeneous catalytic systems for easy recycling.

The first example of hetero-generalized molecular complexes on MOFs was reported by Lin *et al.* in 2011.<sup>16</sup> By successfully incorporating Re<sup>I</sup>(CO)<sub>3</sub>(dcbpy)Cl (dcbpy = (2,2'-bipyridine)-5,5'-dicarboxylic acid, H<sub>2</sub>L) into the porous framework of Zr<sub>6</sub>O<sub>4</sub>(OH)<sub>4</sub>(bpdc)<sub>6</sub> (UiO-67, bpdc = *para*-biphenyldicarboxylic acid), they obtained a Re complex doped MOF heterogeneous photocatalyst active for CO<sub>2</sub> reduction under visible light. The Re doped UiO-67 was synthesized by treating ZrCl<sub>4</sub> with a combination of H<sub>2</sub>bpdc and Re containing H<sub>2</sub>L in DMF at 100 °C. Taking advantage of matching ligand lengths between the ligands bpdc and L, highly crystallized Re doped UiO-67 was obtained, which is iso-structural to the parent framework of UiO-67. The ligand doping level in the MOF is determined to be 4.2% by ICP-MS. Photocatalytic CO<sub>2</sub> reduction of Re-doped UiO-67 was investigated in CO<sub>2</sub>-saturated acetonitrile (MeCN) using triethylamine (TEA) as a sacrificial reducing agent. It was found that the Re-doped MOF selectively reduced CO<sub>2</sub> to CO under visible light. The ratio between CO and H<sub>2</sub> in the product was around 10 during the first 6 h under the reaction conditions (MeCN/TEA = 20/1, saturated with CO<sub>2</sub> gas) and the TON of CO was calculated to be 5.0 after 6 h. No other reduction products like formic acid or methanol were detected. No CO generation was observed in the absence of CO<sub>2</sub> under the same reaction conditions, ruling out the possibility that the detected CO could have resulted from the decomposition of the Re complex. No CO was generated in the dark or on parent UiO-67, confirming that the reduction of CO<sub>2</sub> to CO over the Re-doped UiO-67 is really induced by photocatalysis of the [Re(dcbpy)(CO)<sub>3</sub>Cl] moiety in UiO-67 (Fig. 1).

The recyclability of the Re-doped UiO-67 for photocatalytic CO<sub>2</sub> reduction was also investigated. It was found that the catalyst became inactive in CO generation after two six-hour

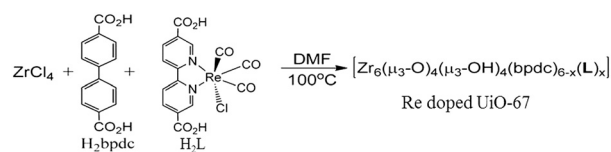


Fig. 1 Synthesis of Re-doped UiO-67. Reprinted with permission from ref. 16.

reaction runs. The total TON of CO over the Re-doped UiO-67 was estimated to be 10.9 after 20 h reaction. The ICP-MS revealed that after 20 h, 43.6% of Re had leached into the supernatant. However, only 3.5% of Zr was detected in the supernatant and the recovered catalyst showed an unchanged XRD pattern of UiO-67. These results suggest that Re leached into solution *via* the detachment of Re-carbonyl moieties from the dcby group and not by the dissolution of the UiO-67 MOF. This is consistent with the observation of the disappearance of the UV-vis peak at 412 nm, a characteristic of the <sup>1</sup>MLCT absorption of the Re(CO)<sub>3</sub>(bpy)Cl species.

In contrast, although the homogeneous Re complex also reduced CO<sub>2</sub> to form CO and a moderate CO-TON of 2.5 was obtained after 6 h reaction, it deactivated very fast. The reaction mixture was almost inactive in the second photocatalytic run. This indicated that the MOF framework can stabilize the homogeneous Re complex. The higher stability of the Re-doped MOF lies in the bimolecular pathway involving a CO<sub>2</sub>-bridged Re dimer, which leads to the deactivation of the Re complex in photocatalytic CO<sub>2</sub> reduction, being able to be inhibited when the Re complex is incorporated into the MOF framework.

Later on, Ryu *et al.* reported the simultaneous incorporation of a Re complex and -NH<sub>2</sub> functionalized BPDC-(NH<sub>2</sub>)<sub>2</sub> (2,2'-diaminobiphenyl-4,4'-dicarboxylic acid) into UiO-67, which led to the formation of Re-MOF-NH<sub>2</sub> with improved photocatalytic activity for CO<sub>2</sub> reduction to produce CO.<sup>17</sup> Re-MOF-NH<sub>2</sub> (X%) (X% refers to -NH<sub>2</sub> groups with respect to the total amount of organic linkers in mol%) was prepared by combining three linkers (Re complex, H<sub>2</sub>BPDC and H<sub>2</sub>BPDC-(NH<sub>2</sub>)<sub>2</sub>) in different ratios and ZrCl<sub>4</sub> in a mixed solution of DMF/acetic acid and heating the mixture at 85 °C for 12 hours. The obtained Re-MOF-NH<sub>2</sub> (X%) with X = 0, 33, 52, 68, and 80 was identified *via* combined experiments using inductively coupled plasma atomic emission spectroscopy (ICP-AES) and <sup>1</sup>H NMR spectroscopy of a digested solution of these samples.

The photocatalytic CO<sub>2</sub> reduction was investigated over the Re-MOF-NH<sub>2</sub> (X%) samples in the presence of TEA under visible light. It was found that the photocatalytic activity over Re-MOF-NH<sub>2</sub> (33%) is the highest, and is about 3-fold higher than that of Re-MOF with no -NH<sub>2</sub> groups. The activity over Re-MOF-NH<sub>2</sub> (33%) was maintained for at least 6 hours, while the homogeneous Re complex deactivated within 1 hour. This can be attributed to both the Re complex and -NH<sub>2</sub> functional groups being covalently bound to the Re-MOF-NH<sub>2</sub> (X%) framework.

Later on, by coating Re-containing UiO-67 onto Ag nanocubes, Yaghi and Yang reported the construction of Ag@Re<sub>3</sub>-MOF with enhanced photocatalytic activity for CO<sub>2</sub> reduction to form CO, which is due to the cooperation of the spatially confined photoactive Re centers and the intensified near-surface electric fields at the surface of Ag nanocubes.<sup>18</sup> A fine balance of proximity between the photoactive centers is required in the Re-containing MOF. The optimal Re<sub>3</sub>-MOF structure, in which each unit cell of the MOF contains 3

ReTCs, was coated on Ag nanocubes to construct Ag@Re<sub>3</sub>-MOF. Due to the synergistic effect played by the plasmonic Ag and photoactive Re centers, the resulting Ag@Re<sub>3</sub>-MOF showed a 7-fold enhancement of CO<sub>2</sub>-to-CO conversion under visible light as well as a long-term stability of up to 48 h (Fig. 2).

In addition to the Re containing photoactive complex, photoactive Rh and Ru containing homogeneous catalysts can also be doped into MOFs for photocatalytic CO<sub>2</sub> reduction. For example, Fontecave *et al.* reported that Cp\* Rh(bpydc)Cl<sub>2</sub> (bpydc = 2,2'-bipyridine-5,5'-dicarboxylic acid) was incorporated into UiO-67 *via* ligand exchange in deionized water at room temperature to afford Cp\* Rh@UiO-67, taking advantage of the similarity between the parent 4,4'-biphenyldicarboxylate (bpdc) linkers and the Rh complex.<sup>19</sup> A synthetically controlled amount of isolated single Rh sites was successfully incorporated into the UiO-67(Zr) framework. The as-obtained Cp\* Rh@UiO-67 showed photocatalytic activity for CO<sub>2</sub> reduction to form HCOO<sup>-</sup> in the presence of a photosensitizer. An optimum Rh loading of ~10% molar is observed. An increased Rh loading leads to a loss of the selectivity to formate due to the decomposition of formate to H<sub>2</sub>. This is the first demonstration of the use of a Rh complex for photocatalytic CO<sub>2</sub> reduction. This study indicated that finding the optimum site density in the design of hybrid solid catalysts is important in order to avoid undesired side reactions.

A Ru<sup>II</sup>-CO complex ([Ru<sup>II</sup>(bpydc)(terpy)(CO)](PF<sub>6</sub>)<sub>2</sub> (terpy refers to 2,2':6',2''-terpyridine)) doped UiO-67 (UiO-67-Ru<sup>II</sup>) was reported by Kitagawa *et al.* prepared *via* a similar ligand exchange strategy between [Ru<sup>II</sup>(bpydc)(terpy)(CO)](PF<sub>6</sub>)<sub>2</sub> and UiO-67.<sup>20</sup> The photocatalytic CO<sub>2</sub> reduction over the as-prepared UiO-67-Ru<sup>II</sup> carried out in CH<sub>3</sub>CN using TEOA as a sacrificial agent and [Ru<sup>II</sup>(bpy)<sub>3</sub>]<sup>2+</sup> as a photosensitizer gave CO, formate and H<sub>2</sub> as the products. It was found that the TON for UiO-67-Ru<sup>II</sup> was comparable to those of H<sub>2</sub>RuCO and [Ru<sup>II</sup>(bpy)(terpy)(CO)](PF<sub>6</sub>)<sub>2</sub>, and is among the highest values reported for PCP-based catalysts when the reaction was carried out under saturated CO<sub>2</sub>. In addition, in low CO<sub>2</sub> concentrations (5% CO<sub>2</sub> diluted with Ar), UiO-67-Ru<sup>II</sup> showed almost unchanged catalytic activity with a TON of 50.3, while the TON over homogeneous [Ru<sup>II</sup>(bpy)(terpy)(CO)](PF<sub>6</sub>)<sub>2</sub>

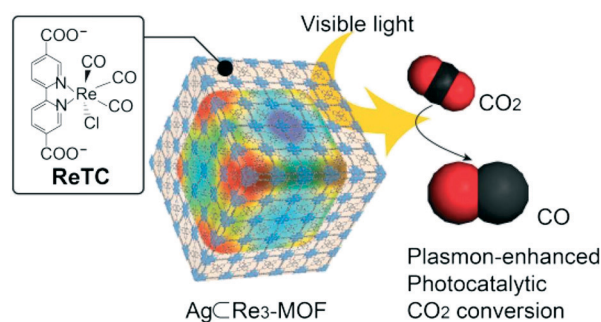


Fig. 2 Visible-light-driven photocatalytic CO<sub>2</sub> reduction over Ag@Re<sub>3</sub>-MOF. Reprinted with permission from ref. 18.

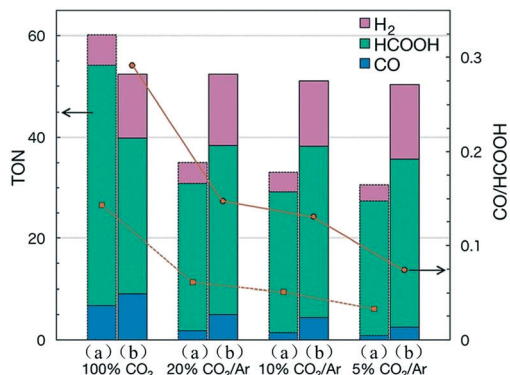


Fig. 3 Photochemical reduction of  $\text{CO}_2$  with (a)  $\text{Ru}^{\text{II}}(\text{bpy})(\text{terpy})(\text{CO})(\text{PF}_6)_2$  and (b)  $\text{Zr-bpdc}/\text{RuCO}$ : left y-axis, catalytic activity (bar graph); right y-axis, product selectivity (line graph). Reprinted with permission from ref. 20.

decreased obviously (TON = 30.6), suggesting the existence of the synergistic effect between the gas adsorption properties of a MOF and the catalytic properties of a molecular catalyst (Fig. 3).

As compared with using ligand exchange to dope photoactive homogeneous complexes into MOFs, the direct construction of supported photoactive metal complexes using the uncoordinated sites on MOFs is appealing since unfavorable interactions between the active species and the solid surface can be minimized in these surface constructed catalysts.<sup>21</sup> By utilizing the open accessible 2,2'-bipyridine units in MOF-253, Li and co-workers prepared a MOF-253-supported Ru-complex ( $\text{MOF-253-Ru}(\text{CO})_2\text{Cl}_2$ ) via the direct coordination of  $[\text{Ru}(\text{CO})_2\text{Cl}_2]$  with the 2,2'-bipyridine units in MOF-253. The photocatalytic  $\text{CO}_2$  reduction over MOF-253- $\text{Ru}(\text{CO})_2\text{Cl}_2$  showed that both  $\text{HCOO}^-$  and CO were produced as the main reduction products, with TON values of 2.9 and 7.1, respectively, after reacting for 8 h. The photocatalytic performance of MOF-253- $\text{Ru}(\text{CO})_2\text{Cl}_2$  can be further improved after modification with  $\text{Ru}(\text{bpy})_2\text{Cl}_2$  to improve its light absorption properties.

Similarly, the post-synthetic metalation of a robust  $\text{Zr}(\text{IV})$ -based MOF with open bpy metal-chelating linkers affords isolated  $\text{Mn}(\text{bpy})(\text{CO})_3\text{Br}$  moieties in the MOF, which is active for photocatalytic  $\text{CO}_2$  reduction to form formate.<sup>22</sup> UiO-67 with open bpy metal-chelating linkers (UiO-67-bpydc) was synthesized by mixing  $\text{ZrCl}_4$ , glacial acetic acid, biphenyl-4,4'-dicarboxylic acid ( $\text{H}_2\text{bpdc}$ ), and 2,2'-bipyridine-5,5'-dicarboxylic acid ( $\text{H}_2\text{bpydc}$ ) in DMF and heating the mixture at 120 °C for 24 h. UiO-67- $\text{Mn}(\text{bpy})(\text{CO})_3\text{Br}$  was prepared by mixing  $\text{Mn}(\text{CO})_5\text{Br}$  and UiO-67-bpydc in  $\text{Et}_2\text{O}$  for 24 h at room temperature. The photocatalytic  $\text{CO}_2$  reduction was carried out in a DMF/TEOA solvent mixture (4:1 v/v) containing  $[\text{Ru}(\text{dmb})_3](\text{PF}_6)_2$  ( $\text{dmb}$  = 4,4'-dimethyl-2,2'-bipyridine) as a photosensitizer and BNAH (1-benzyl-1,4-dihydronicotinamide) as a sacrificial reductant. The resulting UiO-67- $\text{Mn}(\text{bpy})(\text{CO})_3\text{Br}$  was found to be highly active and selective for the photocatalytic reduction of  $\text{CO}_2$  to formate with a TON of 110 in 18 h of catalysis, which exceeds those of the

homogeneous  $\text{Mn}(\text{bpy})(\text{CO})_3\text{Br}$  and  $\text{Mn}(\text{bpydc})(\text{CO})_3\text{Br}$  analogues, as well as many precious-metal-based MOF photocatalysts. The UiO-67 matrix also enhanced the stability of the Mn active sites, allowing them to be reused for up to three cycles.

UiO-66 can also be functionalized via a PSE method using a catechol-functionalized organic linker (catbdc refers to 2,3-dihydroxyterephthalic acid) to produce UiO-66-CAT, which can be further metalated with trivalent metals such as Cr(III) and Ga(III) to afford unprecedented Cr- and Ga-monocatecholato species in robust UiO-66.<sup>23</sup> For the preparation of UiO-66-CAT, UiO-66 was exposed to DMF/ $\text{H}_2\text{O}$  solution containing 2 equiv. of catbdc at 85 °C to give a UiO-66 derivative that contained 34% catbdc and 66% bdc ligand. The metalation of the catechol functionality in UiO-66-CAT carried out in aqueous  $\text{K}_2\text{CrO}_4$  under acidic conditions resulted in a color change from pale yellow to dark brown. ICP-MS confirmed the atomic ratios of 0.25 (Cr/Zr) and 0.26 (Ga/Zr), indicating that 80% of the catbdc was metallated by both Cr and Ga. The photocatalytic  $\text{CO}_2$  reduction over these  $\text{M}(\text{III})$ -monocatecholato functionalized MOFs was carried out in a mixed solution of 4:1 (v/v) MeCN/TEOA in the presence of BNAH, which acts as a reductant for  $\text{CO}_2$  to produce carbonaceous radicals. After 6 h irradiation, the amount of produced HCOOH versus the number of  $\text{M}(\text{III})$ -catecholato sites in each MOF, i.e., the turnover number of HCOOH, was calculated to be ca. 11.22 for UiO-66-CrCAT and ca. 6.14 for UiO-66-GaCAT. Both UiO-66- $\text{M}(\text{III})$ CATs produced negligible amounts of  $\text{H}_2$  and CO. In these  $\text{M}(\text{III})$ -monocatecholato functionalized MOFs, the catbdc organic linkers are responsible for the visible light absorption and charge transfer between the catbdc ligand and metals that occurred through a LMCT mechanism as evidenced by the PL studies. The different activity observed over UiO-66-CrCAT and UiO-66-GaCAT can be ascribed to their different outer shell electronic configurations (Cr(III)  $[\text{Ar}]^3\text{d}^3$  versus Ga(III)  $[\text{Ar}]^3\text{d}^{10}$ ). It is easier for Cr-species to accept electrons than Ga-species due to the higher redox

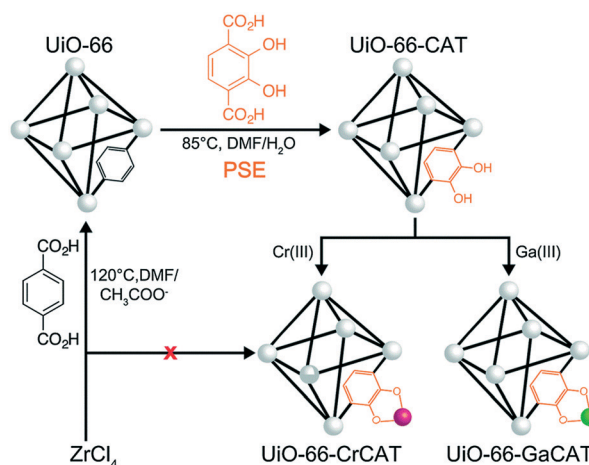


Fig. 4 Preparation of UiO-66-CrCAT and UiO-66-GaCAT through post-synthetic exchange (PSE) and metalation. Reprinted with permission from ref. 23.

potential of Ga(III)/Ga(II) as compared with that of Cr(III)/Cr(II) (Fig. 4).

As compared with MOFs doped with photoactive homogeneous molecular complexes, photoactive MOFs constructed from pure photocatalytic ligands can provide more active sites for photocatalysis. Porphyrins or metalloporphyrins, due to their high light harvesting efficiency and catalytic activity, are important photoactive ligands. The fabrication of porphyrinic metal-organic frameworks (Porph-MOFs) for photocatalysis by using custom-designed porphyrin ligands has also attracted extensive interest due to their rich photo-physical/photochemical properties and tailorable characteristics. For example, PCN-222 (also called MOF-545 or MMPF-6) is a very stable mesoporous zirconium-porphyrin MOF based on tetrakis(4-carboxyphenyl)-porphyrin ( $H_2TCPP$ ). Recently, Jiang *et al.* reported that PCN-222 can be used for photocatalytic  $CO_2$  reduction to produce formate under visible light irradiation.<sup>24</sup> Mechanistic studies based on ultrafast transient absorption spectroscopy and time-resolved photoluminescence spectroscopy revealed the presence of a deep electron trap state in PCN-222, which can effectively inhibit the detrimental, radiative electron-hole recombination. As a result, PCN-222 shows enhanced photocatalytic performance in  $CO_2$  reduction to form formate as compared with the corresponding porphyrin ligand  $H_2TCPP$ . In PCN-222, the ligand  $H_2TCPP$  acts as a visible-light-harvesting unit, while the high  $CO_2$  uptake might facilitate the enrichment of  $CO_2$  molecules around the catalytic  $Zr_6$  centers to enhance the photocatalytic efficiency. This work provides important insights into the design of MOF-based photocatalysts for  $CO_2$  reduction (Fig. 5).

In addition, the porphyrin macrocycle in the Porph-MOFs can be metallated with catalytic active metal sites to promote their photocatalytic performance. For example, Liu *et al.* reported that a Cu-based Porph-MOF ( $S_{Cu}$ ) prepared by the metallation of a Porph-MOF based on TCPP ( $S_p$ ) *via* a PSE strategy exhibits better performance in both  $CO_2$  capture and photocatalytic  $CO_2$  conversion to methanol than Porph-MOFs without Cu.<sup>25</sup> The photocatalytic methanol evolution rate over  $S_{Cu}$  was improved by as high as 7 times as compared

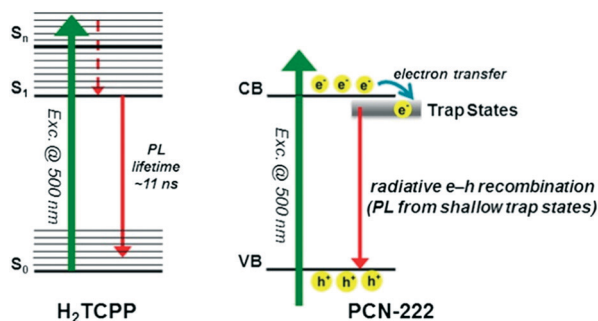


Fig. 5 Mechanisms underlying the photoexcited dynamics involved in  $H_2TCPP$  (left) and PCN-222 (right). Left:  $S_0$ ,  $S_1$ , and  $S_n$  denote the electronic ground state, the first electronically excited state, and a certain high-lying electronically excited state reached by the 500 nm photon, respectively. Right: VB (CB), denoting the valence (conduction) band. Reprinted with permission from ref. 24.

with  $S_p$ , indicating the important role of introduced Cu in the photocatalytic  $CO_2$  reduction. *In situ* FT-IR results suggest that  $CO_2$  can be chemically adsorbed and activated on Cu sites, which played an important role in improving the  $CO_2$  conversion efficiency.

Later on, Zhang *et al.* also reported that the introduction of coordinatively unsaturated Co sites into a Porph-MOF,  $Zr_6O_4(OH)_4(TCPP-H_2)_3$  [MOF-525, TCPP = 4,4',4'',4'''-(porphyrin-5,10,15,20-tetrayl) tetrabenzoate], significantly improved its photocatalytic performance for  $CO_2$  reduction.<sup>26</sup> The Co incorporated MOF-525 (MOF-525-Co) showed much higher activity for  $CO_2$  reduction to form CO and  $CH_4$  as compared with the Zn incorporated MOF-525 (MOF-525-Zn) and parent MOF-525. In metallated Porph-MOFs systems, the introduced metal centers act as the “electron trapping sites” and the directional migration of the photo-generated electrons from porphyrin to these metal active sites helps to supply long-lived electrons for the reduction of  $CO_2$  molecules adsorbed on the MOFs. As compared with Zn, the electron transfer from the porphyrin to Co is more efficient, thus leading to the higher efficiency of MOF-525-Co as compared with MOF-525-Zn (Fig. 6).

In addition to porphyrins and metalloporphyrins, metal complexes can also be used as linkers for the direct construction of photoactive MOFs for  $CO_2$  reduction.  $Ir(ppy)_2(Hdcbpy)$  (HL,  $dcbpy = 2,2'$ -bipyridine-4,4'-dicarboxylate,  $ppy = 2$ -phenylpyridine) is a highly efficient light-harvesting Ir unit. A coordination polymer photocatalyst, Ir-CP, was successfully constructed using the highly efficient light harvesting Ir unit as the building block, which displays remarkable  $CO_2$  photo-reduction efficiency under visible light. Ir-CP was prepared by mixing  $Y(NO_3)_3$ ,  $Ir(ppy)_2(Hdcbpy)$ ,  $H_2O$  and sodium

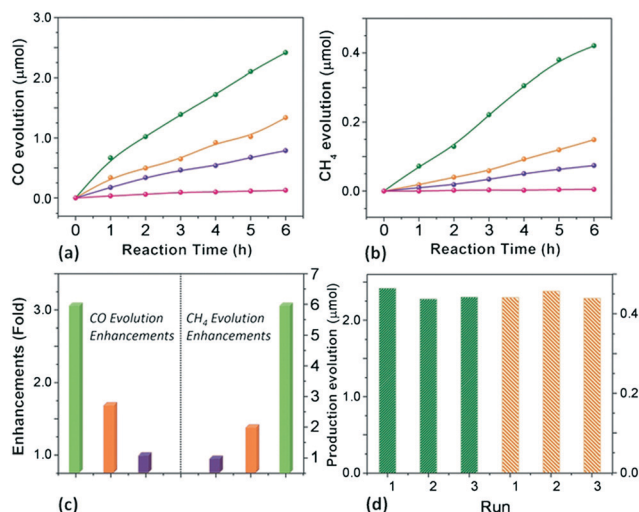


Fig. 6 Time dependent (a) CO and (b)  $CH_4$  evolution over MOF-525-Co (green), MOF-525-Zn (orange), and MOF-525 (purple) photocatalysts and the  $H_2TCPP$  ligand (pink). (c) Enhancement of production evolution over MOF-525-Co (green), MOF-525-Zn (orange), and MOF-525 (purple). (d) Production yield of CO (green) and  $CH_4$  (orange) over the MOF-525-Co photocatalyst as a measure of reproducibility by cycling. Reprinted with permission from ref. 26.

hydroxide solution and heating the mixture in an autoclave at 180 °C for 2 days to yield yellow needle-like crystals.<sup>27</sup> The structure of Ir-CP shows that the Y atom is seven-coordinated by five carboxylate oxygen atoms from different L ligands and two hydroxyl groups to generate a pentagonal bipyramidal coordination geometry. The neighboring Y centers are alternately linked *via* two –OH groups and two carboxylate groups from two L ligands, to give rise to a one-dimensional  $[\text{Y}(\text{OH})_2(\text{CO}_2)_2]\text{N}$  chain structure. The neighbouring chains pack with each other to form a 3D packing supramolecular framework. The presence of the one-dimensional  $[\text{Y}(\text{OH})_2(\text{CO}_2)_2]\text{N}$  chain highlights the stability of the In complex Ir-CP. The absorption spectra show that Ir-CP exhibits light-harvesting in a very broad range, with the absorption edge extended to almost 650 nm, arising from the metal-to-ligand charge transfer (<sup>3</sup>MLCT) and ligand-to-ligand charge transfer (LLCT). PL studies revealed that the luminescence decay can be fitted to a bi-exponential curve with a long lifetime of 29.05 ms for Ir-CP, which is almost four times that of the Ir unit (7.8 ms). This indicates that the formation of the coordination polymer of Ir-CP increases the rigidity and asymmetry of  $[\text{Ir}(\text{ppy})_2(\text{Hdcbpy})]$  and reduces the loss of energy by radiationless decay. The existence of the long lived excited states should be beneficial to efficient photocatalytic reduction of CO<sub>2</sub>. The photocatalytic reduction of CO<sub>2</sub> over Ir-CP in the presence of TEOA as a sacrificial agent revealed that formate was produced as the main product. The amount of formate produced reached 38.0 mmol in 6 h, corresponding to a turnover frequency (TOF) of 118.8 mmol (g of cat.)<sup>-1</sup> h<sup>-1</sup>. Moreover, Ir-CP shows high stability during CO<sub>2</sub> photoreduction.

By adopting an elongated Re-based (bpy)Re(CO)<sub>3</sub>Cl-containing dicarboxylate ligand (bpydb) (bpydb refers to 4,4'-(2,2'-bipyridine-5,5'-diyl)dibenzoate), Wang and Lin *et al.* constructed a highly stable and porous UiO type MOF with a framework formula of  $\{\text{Zr}_6(\text{O})_4(\text{OH})_4[\text{Re}(\text{CO})_3\text{Cl}(\text{bpydb})]_6\}$ .<sup>28</sup> The Re-MOF showed higher TONs for CO than the corresponding homogeneous Re complex, but still underwent decomposition due to partial hydrogenation of the bpy ligand and subsequent Re de-complexation.

Interpenetration in the framework of MOFs was found to influence the stability of the MOFs during the photocatalytic reactions. Using the metalloligands  $[\text{Ru}(5,5\text{-dcbpy})_3]^{4-}$  ( $[\text{Ru-L}_1]^{4-}$ , 5,5'-dcbpy = 2,2'-bipyridine-5,5'-dicarboxylate) and  $[\text{Ru}(4,4'\text{-dcbpy})_2(\text{bpy})]^{2-}$  ( $[\text{Ru-L}_2]^{2-}$ , 4,4'-dcbpy = 2,2'-bipyridine-4,4'-dicarboxylate, bpy = 2,2'-bipyridine) as building blocks, Luo *et al.* rationally designed two Ru-polypyridine containing MOFs, namely,  $\{\text{Cd}_3[\text{Ru-L}_1]_2 \cdot 2(\text{Me}_2\text{NH}_2) \cdot \text{solvent}\}_n$  (Ru-MOF-1) and  $\{\text{Cd}[\text{Ru-L}_2] \cdot 3(\text{H}_2\text{O})\}_n$  (Ru-MOF-2), with non-interpenetrated and interpenetrated structures, respectively, for photocatalytic CO<sub>2</sub> reduction.<sup>29</sup> Ru-MOF-1 was prepared from a mixture of Ru-L<sub>1</sub>, Cd(ClO<sub>4</sub>)<sub>2</sub>·6H<sub>2</sub>O in DMF/H<sub>2</sub>O solution *via* solvothermal heating at 100 °C for 1.5 days. The structure of Ru-MOF-1 possesses 1D channels with large void spaces. The channels are isolated by the enclosed channel walls, which obstruct the structural interpenetration. Ru-

MOF-2 was synthesized by mixing Ru(H<sub>2</sub>dcbpy)<sub>2</sub>Cl<sub>2</sub>, Cd(ClO<sub>4</sub>)<sub>2</sub>·6H<sub>2</sub>O, and bpy in deionized water and adjusting the pH to 10 and the mixture was heated at 180 °C for 3 days. Unlike Ru-MOF-1, Ru-MOF-2 has an interpenetrated framework in its structure. The  $[\text{Ru-L}_2]^{2-}$  metalloligand linked to Cd(n) centers results in a network, which exhibits a large 3D void space to accommodate a second framework *via* interpenetration, leading to a 2-fold interpenetrating structure for Ru-MOF-2. The two interpenetrated frameworks are stabilized by strong  $\pi$ -stacking interactions between the dcbpy<sup>2-</sup> ligands of the neighboring nets. Both MOFs exhibit very broad absorption bands between 400 and 650 nm, assignable to the singlet metal-to-ligand charge transfer (<sup>1</sup>MLCT) of Ru metalloligands. Both Ru-MOF-1 and Ru-MOF-2 show photocatalytic activity for CO<sub>2</sub> reduction to form formate under visible light in the presence of TEOA as a sacrificial agent. In 6 h, the levels of formate produced over Ru-MOF-1 and Ru-MOF-2 were comparable and reached 16.1 and 17.2 mol over Ru-MOF-1 and Ru-MOF-2, respectively. However, prolonged photocatalytic reaction revealed that Ru-MOF-2 shows higher stability than Ru-MOF-1. Ru-MOF-2 maintains its photocatalytic activity in the second 6 h of reaction time. However, Ru-MOF-1 gradually became inactive during the same period. In addition, both the XRD and SEM confirm that the framework of Ru-MOF-1 collapsed, while Ru-MOF-2 can maintain its structure during the photocatalytic reaction. The higher durability observed over Ru-MOF-2 as compared with Ru-MOF-1 suggests that making use of interpenetration could be an effective strategy to fabricate highly stable MOF-based photocatalysts (Fig. 7).

The construction of hierarchical nano-architectures has been widely adopted in inorganic nanomaterials for nanoparticles to retain their high activity and exhibit higher stability for recycling. Luo *et al.* reported the fabrication of mono-disperse hierarchical nanoflowers of a Ru-MOF,  $\{\text{Cd}_2[\text{Ru}(\text{dcbpy})_3] \cdot 12\text{H}_2\text{O}\}_n$  (dcbpy = 2,2'-bipyridine-4,4'-dicarboxylate), *via* a facile surfactantless solvothermal method.<sup>30</sup> By controlling the concentration of the reactants, the morphologies of the Ru-MOF can be easily tuned from sub-millimeter scale flakes to micro-scale nanoflowers. These nano-flowers of Ru-MOF are applied in photocatalytic CO<sub>2</sub> reduction and exhibit good stability during the photocatalytic reaction.

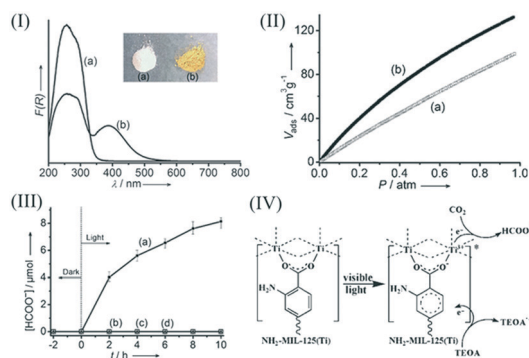


Fig. 7 Photocatalytic CO<sub>2</sub> reduction over two Ru-MOFs. Reprinted with permission from ref. 29.

### 3. CO<sub>2</sub> reduction initiated by photoactive metal nodes

MOFs are constructed from metal or metal cluster nodes interconnected with multi-dentate organic linkers. In addition to photoactive ligands, metal nodes in MOFs can also initiate photocatalysis. Based on the pioneering studies by Zecchina, García and Majima on MOF-5, a widely studied Zn-containing MOF material, it is currently widely accepted that the metal nodes can act as semiconductor QDs, while the organic linkers can act as the antenna to sensitize these QDs.<sup>4</sup> As compared with traditional inorganic semiconductors, it is easier to tune the light absorption properties of MOFs to make effective use of solar light by modifications on the metal ions or the organic ligands, taking advantage of the versatile coordination modes of the metal ions and the availability of different organic ligands. Photocatalytic CO<sub>2</sub> reduction initiated by the metal nodes in the MOFs has also been reported (Fig. 8).

In 2012, Li and co-workers first reported that NH<sub>2</sub>-MIL-125(Ti), a Ti-containing MOF material, can photocatalytically reduce CO<sub>2</sub> to form HCOO<sup>-</sup> under visible light irradiation.<sup>6a</sup> By replacing the 1,4-benzene dicarboxylate (BDC) linker in MIL-125(Ti), which is constructed from TiO<sub>5</sub>(OH) octahedra and BDC, with 2-aminoterephthalic acid (H<sub>2</sub>ATA), they successfully obtained iso-structural amine functionalized NH<sub>2</sub>-MIL-125(Ti). The presence of an amine group in NH<sub>2</sub>-MIL-125(Ti) results in extra light absorption in the visible region and enhances its adsorption capacity toward CO<sub>2</sub>. The photocatalytic CO<sub>2</sub> reduction over NH<sub>2</sub>-MIL-125(Ti) in the presence of TEOA as a sacrificial agent revealed that HCOO<sup>-</sup> was produced as the only product under visible light irradiation, and about 8.14 μmol of HCOO<sup>-</sup> was formed after reacting for 10 h. The isotopic <sup>13</sup>CO<sub>2</sub> reaction confirmed that the as-formed HCOO<sup>-</sup> originated from the reduction of CO<sub>2</sub> over NH<sub>2</sub>-MIL-125(Ti). ESR results reveal that the photo-generated Ti<sup>3+</sup> moiety *via* the LMCT is responsible for the formation of HCOO<sup>-</sup>.



**Fig. 8** (I) UV-vis spectra of (a) MIL-125(Ti) and (b) NH<sub>2</sub>-MIL-125(Ti); (II) CO<sub>2</sub> adsorption isotherms (1 atm, 273 K) of (a) MIL-125(Ti) (□) and (b) NH<sub>2</sub>-MIL-125(Ti) (■); (III) the amount of HCOO<sup>-</sup> produced as a function of the time of irradiation over (a) NH<sub>2</sub>-MIL-125(Ti) (■), (b) MIL-125(Ti) (□), (c) a mixture of TiO<sub>2</sub> and H<sub>2</sub>ATA (19 mg + 32 mg) (○) and (d) visible light irradiation without a sample (▲); (IV) proposed mechanism for the photocatalytic CO<sub>2</sub> reduction over NH<sub>2</sub>-MIL-125(Ti) under visible light irradiation. Reprinted with permission from ref. 6a.

Although the catalytic efficiency over NH<sub>2</sub>-MIL-125(Ti) is low, this work is the first demonstration that the metal nodes in MOFs can be used in photocatalytic CO<sub>2</sub> reduction, which opens a new perspective for the development of noble-metal-free MOF-based photocatalysts for CO<sub>2</sub> reduction.

Later on, Li and co-workers investigated the photocatalytic CO<sub>2</sub> reduction over amine-functionalized NH<sub>2</sub>-Uio-66(Zr), a Zr-containing MOF that was previously reported by García *et al.* for hydrogen evolution under UV light irradiation. It was found that CO<sub>2</sub> can be reduced to form HCOO<sup>-</sup> over visible light irradiated NH<sub>2</sub>-Uio-66(Zr) with the involvement of a Zr<sup>3+</sup> moiety generated from the LMCT. The activity for photocatalytic CO<sub>2</sub> reduction over NH<sub>2</sub>-Uio-66(Zr) is even higher than that over NH<sub>2</sub>-MIL-125(Ti).<sup>31</sup> These studies indicate that MOFs containing redox-active metal clusters can be promising materials for photocatalytic CO<sub>2</sub> reduction and their performance are influenced by the composition and structure of the MOF materials.

The studies on the photocatalytic CO<sub>2</sub> reduction over NH<sub>2</sub>-MIL-125(Ti) and NH<sub>2</sub>-Uio-66(Zr) revealed that the redox metal centers are the actual catalytically active species. However, the generation of Ti<sup>3+</sup> in NH<sub>2</sub>-MIL-125(Ti) and Zr<sup>3+</sup> in NH<sub>2</sub>-Uio-66(Zr) involves light excitation on the organic linkers followed by a LMCT process. Direct excitation on the metal oxo clusters on the MOF materials would be more efficient for the generation of catalytically active metal centers and therefore beneficial to the photocatalytic CO<sub>2</sub> reaction. Since most of the Fe-based MOF materials already reported are visible-light-responsive due to the existence of extensive iron oxo clusters, Li and co-workers later reported the visible-light-induced photocatalytic CO<sub>2</sub> reduction over a series of Fe-containing MOFs, including MIL-101(Fe), MIL-53(Fe) and MIL-88B(Fe).<sup>6b</sup> It was found that all three Fe-MOFs are capable of reducing CO<sub>2</sub> to form HCOO<sup>-</sup> under visible light irradiation. Among the three Fe-based MOFs investigated, MIL-101(Fe) showed the highest activity and the amount of HCOO<sup>-</sup> produced in 8 h reached 59 mol. The higher performance of MIL-101(Fe) as compared with MIL-53(Fe) and MIL-88(Fe) can be ascribed to the presence of unsaturated Fe coordination sites, as confirmed by the *in situ* FT-IR. Amine-functionalization on the three Fe-MOFs led to obviously higher activity than those of the un-functionalized ones. For example, the amount of HCOO<sup>-</sup> formed reached 178 mol in 8 h over NH<sub>2</sub>-MIL-101(Fe), which is about 3.0-fold greater in comparison with that for the parent MIL-101(Fe) under similar conditions. The highest QE at 450 nm observed over NH<sub>2</sub>-MIL-101(Fe) is determined to be 1.3 × 10<sup>-4</sup>. Such an enhancement in photocatalytic performance can be attributed to the existence of dual excitation pathways: *i.e.*, excitation of the NH<sub>2</sub> functionality followed by electron transfer to the Fe center in addition to the direct excitation of Fe-O clusters. The studies on the photocatalytic CO<sub>2</sub> reduction over these Fe-containing MOFs not only provide a better understanding of the photocatalytic CO<sub>2</sub> reduction over MOF-based materials but also demonstrate great opportunities to design MOFs with inexpensive elements for CO<sub>2</sub> conversion (Fig. 9).

Photoactive metal nodes in MOFs that can drive photocatalytic CO<sub>2</sub> reduction under visible light are still limited and only restricted to Ti-, Zr- and Fe-based MOFs. Since these kinds of MOF-based photocatalysts share similarity to semiconductor-based photocatalysts, strategies used to improve the performance of semiconductor-based photocatalysts can also be applied in these kinds of MOF-based photocatalysts. Therefore, MOFs with strong light absorption in the visible light region that can also undergo fast charge separation and migration are highly suited to achieve efficient photocatalysis. The use of ligands with broad light absorption in the visible light region is an important strategy to improve light absorption of MOF-based photocatalysts, while metal substitution or doping on MOFs can improve the efficiency of charge separation in MOFs. All these strategies can be readily achieved on MOFs due to the high tunability of the composition and structures of MOFs and their peculiar characteristics.

For example, to enhance the light absorption properties of NH<sub>2</sub>-UiO-66(Zr), Li *et al.* partially substituted the ATA in NH<sub>2</sub>-UiO-66(Zr) with 2,5-diaminoterephthalic acid (H<sub>2</sub>DTA) during the preparation process to obtain mixed NH<sub>2</sub>-UiO-66(Zr) with both ATA and DTA linkers (mixed NH<sub>2</sub>-UiO-66(Zr)).<sup>31</sup> It was found that the as-obtained mixed NH<sub>2</sub>-UiO-66(Zr) is much more active for CO<sub>2</sub> reduction as compared with bare NH<sub>2</sub>-UiO-66(Zr), with about 50% higher amount of HCOO<sup>-</sup> produced under similar conditions. Control experiments revealed that the extra absorption introduced by the amine functionalization on the mixed NH<sub>2</sub>-UiO-66(Zr) is responsible for its improved photocatalytic CO<sub>2</sub> reduction performance.

In addition to modifications on organic linkers, post-synthetic exchange (PSE) of the metal centers on MOFs has also been applied. For example, partial substitution of Zr in NH<sub>2</sub>-UiO-66(Zr) by a Ti moiety *via* a PSE method led to the mixed metal NH<sub>2</sub>-UiO-66(Zr/Ti) with enhanced photocatalytic performance for CO<sub>2</sub> reduction under visible light irradiation.<sup>32</sup> Inductively coupled plasma optical emission spectrometry (ICP-OES) analysis of this NH<sub>2</sub>-UiO-66(Zr/Ti) revealed that about 53.4% of Zr in the NH<sub>2</sub>-UiO-66(Zr) framework was substituted by Ti. The introduced Ti moieties act as electron mediators to facilitate the electron transfer from the excited organic linker ATA to the Zr–O cluster to form Zr<sup>III</sup>, the actual active species for the CO<sub>2</sub> reduction, and contribute to the enhanced photocatalytic activity, which is confirmed by the

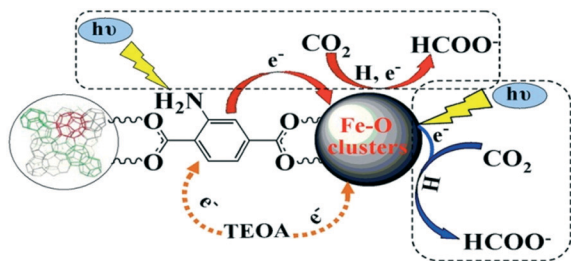


Fig. 9 Dual excitation pathways over amino-functionalized Fe-based MOFs. Reprinted with permission from ref. 33.

electron spin resonance (ESR) analysis and density functional theory (DFT). Evidence supporting Ti acting as a mediator in the photoinduced electron transfer is also provided by transient absorption spectroscopy.<sup>33</sup> Later on, Cohen *et al.* extended this strategy to the preparation of mixed-metal, mixed ligand MOFs based on NH<sub>2</sub>-UiO-66(Zr) for enhanced CO<sub>2</sub> reduction by combining Zr-by-Ti exchange with the partial substitution of ligands to enhance the light absorption.<sup>34</sup> The facile realization of metal substitution in MOFs and their structural diversity would allow us to develop a variety of MOF-based photocatalysts with the desired performance in a more controllable way (Fig. 10).

Doping of noble metals into semiconductor-based photocatalysts has already been proved to be an effective method to improve their photocatalytic activity. Although the doping of suitable noble metal nanoparticles into MOFs can also increase their photocatalytic performance by improving the separation of the charge carriers, different noble metals may have different effects on the photocatalytic CO<sub>2</sub> reduction over MOF materials. For example, it was found that Pt-doped NH<sub>2</sub>-MIL-125(Ti) prepared *via* H<sub>2</sub> heat treatment shows enhanced photocatalytic performance for CO<sub>2</sub> reduction to form HCOO<sup>-</sup>.<sup>35</sup> The promoting effect played by Pt on the photocatalytic CO<sub>2</sub> reduction over NH<sub>2</sub>-MIL-125(Ti) is believed to be related to the spillover of the as-formed hydrogen from the noble metal to the Ti center in Pt/NH<sub>2</sub>-MIL-125(Ti) and thus promote the formation of Ti<sup>III</sup>, the actual active species for the photocatalytic CO<sub>2</sub> reduction. However, similar Au doping on NH<sub>2</sub>-MIL-125(Ti) has a negative effect on HCOO<sup>-</sup> formation, while promoting the photocatalytic hydrogen evolution. This work clearly illustrates the different roles of noble metals on MOFs in photocatalysis and the demonstrated hydrogen spillover mechanism observed over the Pt/MOF system provides great opportunities for their applications in photocatalytic reactions involving hydrogen as a reactant, like hydrogenation reactions.

The photoactive metal clusters can also couple with the photoactive organic ligands in a single MOF material for cooperated photocatalytic CO<sub>2</sub> reduction. For example, NNU-28 is a microporous robust zirconium metal–organic framework (Zr-MOF) constructed using a visible light responsive organic ligand derived from an anthracene group.<sup>36</sup> NNU-28 shows excellent chemical and thermal stability, high CO<sub>2</sub>

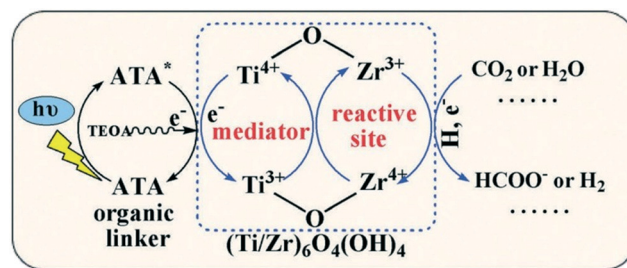


Fig. 10 Proposed enhanced mechanism for the photocatalytic reactions over NH<sub>2</sub>-UiO-66(Zr/Ti). Reprinted with permission from ref. 34.

uptake, broad-band visible light absorption and efficient photo-induced charge generation, which makes it suitable for photocatalytic CO<sub>2</sub> reduction under visible light. It was found that NNU-28 is highly efficient for visible-light-driven CO<sub>2</sub> reduction with a formate formation rate of 183.3 mmol h<sup>-1</sup> mmol<sup>-1</sup> MOF. The photocatalytic experiments and electron paramagnetic resonance (EPR) studies reveal that both the inorganic building unit Zr<sub>6</sub> oxo cluster and the anthracene-based ligand contribute to CO<sub>2</sub> photoreduction (Fig. 11).

#### 4. CO<sub>2</sub> reduction promoted by MOFs in a hybrid photocatalytic system

In addition to being used directly as photocatalysts, MOFs can also act as cocatalysts for photocatalytic CO<sub>2</sub> reduction in a nanocomposite, in which MOFs either promote the kinetic processes of the catalytic reactions or enhance the CO<sub>2</sub> adsorption, while the other component (*e.g.*, dyes, semiconductors *etc.*) in the nanocomposite acts as the photo-harvesting part to form light-generated charge carriers.

Co-ZIF-9 is a porous crystalline structure composed of cobalt(II) ions linked to benzimidazole (bIm) ligands, merging the catalytic functions of cobalt and imidazole motifs. The use of Co-ZIF-9 as a co-catalyst for the photocatalytic CO<sub>2</sub> reduction was first reported by Wang *et al.* in 2014.<sup>37</sup> The photocatalytic reaction was carried out using [Ru(bpy)<sub>3</sub>]Cl<sub>2</sub>·6H<sub>2</sub>O (bpy refers to 2,2'-bipyridine) as a photosensitizer, Co-ZIF-9 as a co-catalyst and TEOA as a sacrificial electron donor under visible light irradiation. Different from other MOF-based photocatalysis processes, CO instead of HCOO<sup>-</sup> was produced as the main product along with the formation of H<sub>2</sub>. Control experiments using other MOFs including Co-MOF-74, Mn-MOF-74, NH<sub>2</sub>-Uio-66(Zr) and Zn-ZIF-8 to replace Co-ZIF-9 led to decreased photocatalytic activity, indicating that the synergistic effect between the cobalt and benzimidazole entities in Co-ZIF-9 can facilitate the CO<sub>2</sub> reduction reaction. Although relatively high catalytic efficiency was achieved over this photocatalytic system, the selectivity to CO was quite low (CO/H<sub>2</sub> = 1.4) and the photobleaching of the dye leads to the decrease of catalytic activity. To achieve higher performance, Wang *et al.* also extended the use of Co-ZIF-9 as a co-catalyst for CO<sub>2</sub> reduction by coupling it with several semiconductor photocatalysts, like g-C<sub>3</sub>N<sub>4</sub>,<sup>38</sup> CdS,<sup>39</sup> as light harvesters. Benefiting from the high visible light photocatalytic activity of CdS, the CdS/Co-ZIF-9 hybrid system

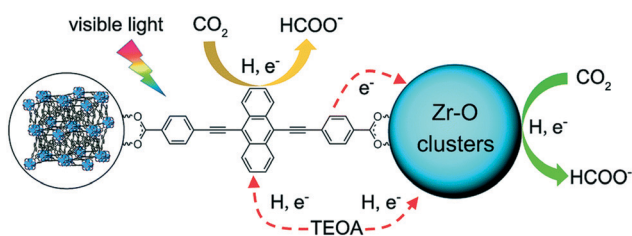


Fig. 11 A scheme of dual photocatalytic routes for visible-light-driven CO<sub>2</sub> reduction in NNU-28. Reprinted with permission from ref. 36.

attained a high apparent quantum yield (AQY) of 1.93% for photocatalytic CO<sub>2</sub> reduction at 420 nm monochromatic irradiation. However, a main drawback of these Co-ZIF-9 hybrid systems involves the use of bpy as an assistant electron mediator during photocatalytic CO<sub>2</sub> reduction (Fig. 12).

Taking advantage of the high adsorption capacity of MOFs toward CO<sub>2</sub> and the high stability and good photocatalytic ability of TiO<sub>2</sub>, MOF/TiO<sub>2</sub> hybrid systems have been extensively studied for photocatalytic CO<sub>2</sub> reduction. For example, Xiong *et al.* synthesized a Cu<sub>3</sub>(BTC)<sub>2</sub>@TiO<sub>2</sub> core@shell structure (Cu<sub>3</sub>(BTC)<sub>2</sub> named HKUST-1, BTC = benzene-1,3,5-tricarboxylate) by coating a nanocrystalline TiO<sub>2</sub> shell onto the Cu<sub>3</sub>(BTC)<sub>2</sub> core.<sup>40</sup> The as-obtained Cu<sub>3</sub>(BTC)<sub>2</sub>@TiO<sub>2</sub> hybrid system showed a five-fold enhancement in its photocatalytic activity for CO<sub>2</sub> reduction to produce CH<sub>4</sub>, as well as significantly promoted selectivity to CH<sub>4</sub> as compared with the pristine TiO<sub>2</sub>. Ultrafast spectroscopy characterization indicated that the photo-generated electrons produced from the photoexcitation of the TiO<sub>2</sub> shell could effectively transfer to the Cu<sub>3</sub>(BTC)<sub>2</sub> core, improving the separation of photo-generated electron-hole pairs on TiO<sub>2</sub>,<sup>41</sup> and providing energetic electrons to reduce CO<sub>2</sub> molecules adsorbed on the Cu<sub>3</sub>(BTC)<sub>2</sub> co-catalyst. Also, a similar HKUST-1/TiO<sub>2</sub> nanocomposite in micrometer-sized droplets prepared *via* a rapid aerosol route was found to show enhanced photocatalytic CO<sub>2</sub> reduction as compared with TiO<sub>2</sub>. Li *et al.* also reported the integration of CPO-27-Mg (Mg<sub>2</sub>(DOBDC), DOBDC = 2,5-

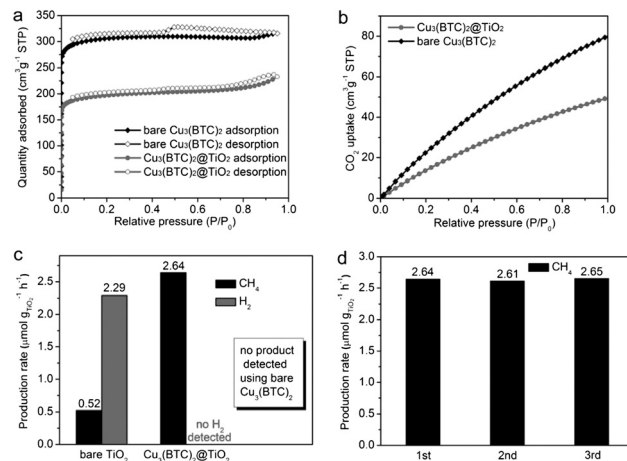


Fig. 12 (a) N<sub>2</sub> adsorption-desorption isotherms and (b) CO<sub>2</sub> adsorption behaviors for Cu<sub>3</sub>(BTC)<sub>2</sub>@TiO<sub>2</sub> core-shell structures and bare Cu<sub>3</sub>(BTC)<sub>2</sub>, respectively. The data are plotted based on the total weights of materials. (c) Production yields of CH<sub>4</sub> and H<sub>2</sub> from CO<sub>2</sub> using Cu<sub>3</sub>(BTC)<sub>2</sub>@TiO<sub>2</sub> core-shell structures as photocatalysts under UV irradiation for 4 h, in reference to bare TiO<sub>2</sub> nanocrystals calculated using the weight of photoactive TiO<sub>2</sub>. Bare Cu<sub>3</sub>(BTC)<sub>2</sub> microcrystals were also used as a reference. 100 mg bare TiO<sub>2</sub>, 200 mg bare Cu<sub>3</sub>(BTC)<sub>2</sub>, and 300 mg Cu<sub>3</sub>(BTC)<sub>2</sub>@TiO<sub>2</sub> hybrid structures were used in the measurements. The samples were carefully pretreated to remove any carbon contaminants. No CO or alcohol products were found for any samples, and formation of O<sub>2</sub> was observed for the oxidation. (d) Production yields of CH<sub>4</sub> with the Cu<sub>3</sub>(BTC)<sub>2</sub>@TiO<sub>2</sub> photocatalyst in recycling tests. Reprinted with permission from ref. 40.

dioxido-1,4-benzenedicarboxylate), a  $Mg^{2+}$  based metal–organic framework which shows the highest  $CO_2$  uptake among the already reported MOF materials, with  $TiO_2$  to form a CPO-27-Mg/ $TiO_2$  nanocomposite for photocatalytic  $CO_2$  reduction.<sup>42</sup> Due to the high adsorption capacity toward  $CO_2$  and the existence of open alkaline metal sites in CPO-27-Mg, the as-obtained CPO-27-Mg/ $TiO_2$  nanocomposite exhibited enhanced performance for the photocatalytic  $CO_2$  reduction to form CO and  $CH_4$  and the competitive reduction of  $H_2O$  to  $H_2$  was totally inhibited. This study highlights the promising prospect of incorporating MOFs with open alkaline metal sites into semiconductors for artificial  $CO_2$  photo-conversion.

In addition to  $TiO_2$ ,  $Zn_2GeO_4$  has also been coupled with MOFs for photocatalytic  $CO_2$  reduction. In 2013, Liu *et al.* reported the growth of ZIF-8 nanoparticles on  $Zn_2GeO_4$  nanorods for photocatalytic  $CO_2$  reduction.<sup>43</sup> It was found that the resulting ZIF-8/ $Zn_2GeO_4$  nanocomposites converted  $CO_2$  to produce  $CH_3OH$  in aqueous solution and exhibited higher photocatalytic activity as compared to bare  $Zn_2GeO_4$  nanorods. The authors also attributed the promoted photocatalytic performance of ZIF-8/ $Zn_2GeO_4$  to the strong  $CO_2$  adsorption ability of ZIF-8.

Photoactive MOFs like  $NH_2$ -UiO-66 can also be integrated with inorganic semiconductors to form heterojunction nanocomposites. The presence of  $NH_2$ -UiO-66(Zr) in a nanocomposite not only enhances the adsorption toward  $CO_2$  but also helps to promote the separation of the photo-generated charge carriers *via* the formation of the semiconductor–MOF heterojunction. For example, Petit *et al.* reported the construction of  $NH_2$ -UiO-66(Zr)/ $TiO_2$  nanocomposites, which show enhanced photocatalytic activity for  $CO_2$  reduction to form CO as compared with their single components.<sup>44</sup> As revealed by transient absorption spectroscopy (TAS), the improved photocatalytic performance was attributed to the enhanced abundance of long lived charge carriers, which occurred due to the effective charge transfer *via* the MOF/semiconductor interface.  $NH_2$ -UiO-66 was also found to integrate with  $Cd_{0.2}Zn_{0.8}S$  solid solution for enhanced photocatalytic  $CO_2$  reduction to produce  $CH_3OH$ .<sup>45</sup>

## 5. Outlook and prospects

This review summarized the recent progress in using MOFs for photocatalytic  $CO_2$  reduction, in which MOFs either act directly as the photocatalysts or as components to promote  $CO_2$  reduction in a hybrid photocatalytic system. Although still in their early stage, these works demonstrate that MOF-based materials hold great promise for applications in the field of  $CO_2$  reduction. However, there are some limitations in using MOFs in this field. First, the already reported performance for  $CO_2$  reduction over MOF-based materials is still very limited and with a very low turnover number, which in part can be attributed to the poor electroconductivity of MOFs and the inaccessibility of all the catalytic active sites to the reactants. Second, most of the MOFs are not as stable as semiconductor-based photocatalysts, especially in water or

under UV light irradiation. Third, the mechanism for photocatalytic  $CO_2$  reduction over MOFs is still unclear. No studies on the crystal size effect of MOFs on their performance have ever been demonstrated. Fourth, the high product cost which may arise from the low-throughput production of MOFs may restrict their application. Last but not the least, most of the photocatalytic  $CO_2$  reduction reactions were performed in organic solvents with the presence of sacrificial agents such as TEOA and TEA, which is not economical and environmentally friendly. It would be ideal if the  $CO_2$  conversion can be performed in water or coupled with an organic oxidation process, which can convert  $CO_2$  to fine chemicals.

To address the above problems, the following efforts should be made in the future. First is the elucidation of the photocatalytic mechanism of  $CO_2$  reduction over MOF-based materials and the composition–structure–performance relationship, which can lead to the rational design and development of stable MOFs with the optimum composition and structure for  $CO_2$  reduction. Transient absorption techniques may provide useful information on the nature, lifetimes and reactivity of the transient species involved in the reactions, and thus could be useful for the understanding of the photocatalytic mechanism. Second is the rational design and development of MOF-based nanocomposites by effectively combining MOF-based photocatalysis with molecular (photo) catalysis and MOF-based photocatalysis with metal catalysis/organocatalysis to couple photocatalytic  $CO_2$  reduction with the oxidation of water or organics to convert  $CO_2$  into valuable organics without the use of sacrificial agents. This is a promising and sustainable strategy for  $CO_2$  conversion which requires more extensive future studies.

## Conflicts of interest

There are no conflicts to declare.

## Acknowledgements

This work was supported by the 973 Program (2014CB239303), NSFC (21273035), the National Key Technologies R&D Program of China (2014BAC13B03) and the Independent Research Project of the State Key Laboratory of Photocatalysis on Energy and Environment (2014A03). Z. L. thanks the Award Program for Minjiang Scholar Professorship for financial support.

## Notes and references

- (a) D. L. Ashford, M. K. Gish, A. K. Vannucci, M. K. Brennaman, J. L. Templeton, J. M. Papanikolas and T. J. Meyer, *Chem. Rev.*, 2015, **115**, 13006–13049; (b) J. L. White, M. F. Baruch, J. E. Pander, Y. Hu III, I. C. Fortmeyer, J. E. Park, T. Zhang, K. Liao, J. Gu, Y. Yan, T. W. Shaw, E. Abelev and A. B. Bocarsly, *Chem. Rev.*, 2015, **115**, 12888–12935; (c) Y. Yamazaki, H. Takeda and O. Ishitani, *J. Photochem. Photobiol., C*, 2015, **25**, 106–137; (d) W. G. Tu, Y. Zhou and Z. G. Zou, *Adv. Mater.*, 2014, **26**, 4607–4626; (e) X. Liu, S.

- Inagaki and J. L. Gong, *Angew. Chem., Int. Ed.*, 2016, 55, 14924–14950; (f) X. X. Chang, T. Wang and J. L. Gong, *Energy Environ. Sci.*, 2016, 9, 2177–2196; (g) M. Marszewski, S. W. Cao, J. G. Yu and M. Jaroniec, *Mater. Horiz.*, 2015, 2, 61–278.
- 2 (a) H. C. Zhou, J. R. Long and O. M. Yaghi, *Chem. Rev.*, 2012, 112, 673–674; (b) H. Furukawa, K. E. Cordova, M. O’Keeffe and O. M. Yaghi, *Science*, 2013, 341, 1230444; (c) L. E. Kreno, K. Leong, O. K. Farha, M. Allendorf, R. P. Van Duyne and J. T. Hupp, *Chem. Rev.*, 2012, 112, 1105–1125; (d) H. C. Zhou and S. Kitagawa, *Chem. Soc. Rev.*, 2014, 43, 5415–5418; (e) P. Horcajada, R. Gref, T. Baati, P. K. Allan, G. Maurin, P. Couvreur, G. Ferey, R. E. Morris and C. Serre, *Chem. Rev.*, 2012, 112, 1232–1268; (f) M. P. Suh, H. J. Park, T. K. Prasad and D. W. Lim, *Chem. Rev.*, 2012, 112, 782–835; (g) Y. He, B. Li, M. O’Keeffe and B. Chen, *Chem. Soc. Rev.*, 2014, 43, 5618–5656; (h) B. Van de Voorde, B. Bueken, J. Denayer and D. De Vos, *Chem. Soc. Rev.*, 2014, 43, 5766–5788; (i) J. Lee, O. K. Farha, J. Roberts, K. A. Scheidt, S. T. Nguyen and J. T. Hupp, *Chem. Soc. Rev.*, 2009, 38, 1450–1459; (j) D. Farrusseng, S. Aguado and C. Pinel, *Angew. Chem., Int. Ed.*, 2009, 48, 7502–7513; (k) H. L. Jiang and Q. Xu, *Chem. Commun.*, 2011, 47, 3351–3370; (l) J. R. Li, J. Sculley and H. C. Zhou, *Chem. Rev.*, 2012, 112, 869–932; (m) A. Corma, H. Garcia and F. X. Llabrés i Xamena, *Chem. Rev.*, 2010, 110, 4606–4655; (n) W. Y. Gao, M. Chrzanowski and S. Q. Ma, *Chem. Soc. Rev.*, 2014, 43, 5841–5866; (o) W. M. Xuan, C. F. Zhu, Y. Liu and Y. Cui, *Chem. Soc. Rev.*, 2012, 41, 1677–1695; (p) Y. B. Huang, J. Liang, X. S. Wang and R. Cao, *Chem. Soc. Rev.*, 2017, 46, 126–157.
- 3 (a) J. Gascon, A. Corma, F. Kapteijn and F. X. Llabrés i Xamena, *ACS Catal.*, 2014, 4, 361–378; (b) T. Zhang and W. Lin, *Chem. Soc. Rev.*, 2014, 43, 5982–5993.
- 4 (a) S. Bordiga, C. Lamberti, G. Ricchiardi, L. Regli, F. Bonino, A. Damin, K. P. Lillerud, M. Bjorgen and A. Zecchina, *Chem. Commun.*, 2004, 2300–2301; (b) M. Alvaro, E. Carbonell, B. Ferrer, F. X. Llabrés i Xamena and H. Garcia, *Chem. – Eur. J.*, 2007, 13, 5106–5112; (c) T. Tachikawa, J. R. Choi, M. Fujitsuka and T. Majima, *J. Phys. Chem. C*, 2008, 112, 14090–14101.
- 5 (a) C. Wang, Z. Xie, K. E. deKrafft and W. Lin, *J. Am. Chem. Soc.*, 2011, 133, 13445–13454; (b) T. Toyao, M. Saito, S. Dohshi, K. Mochizuki, M. Iwata, H. Higashimura, Y. Horiuchi and M. Matsuoka, *Chem. Commun.*, 2014, 50, 6779–6781.
- 6 (a) Y. Fu, D. Sun, Y. Chen, R. Huang, Z. Ding, X. Fu and Z. Li, *Angew. Chem., Int. Ed.*, 2012, 51, 3364–3367; (b) D. K. Wang, R. K. Huang, W. J. Liu, D. R. Sun and Z. H. Li, *ACS Catal.*, 2014, 4, 4254–4260; (c) A. Crake, *Mater. Sci. Technol.*, 2016, 115, 33–52.
- 7 (a) K. Meyer, M. Ranocchiari and J. A. van Bokhoven, *Energy Environ. Sci.*, 2015, 8, 1923–1937; (b) C. G. Gomes Silva, I. Luz, F. X. Llabrés i Xamena, A. Corma and H. Garcia, *Chem. – Eur. J.*, 2010, 16, 11133–11138; (c) Y. Horiuchi, T. Toyao, M. Saito, K. Mochizuki, M. Iwata, H. Higashimura, M. Anpo and M. Matsuoka, *J. Phys. Chem. C*, 2012, 116, 20848–20853; (d) M. A. Nasalevich, R. Becker, E. V. Ramos-Fernandez, S. Castellanos, S. L. Veber, M. V. Fedin, F. Kapteijn, J. N. H. Reek, J. I. van der Vlugt and J. Gascon, *Energy Environ. Sci.*, 2015, 8, 364–375; (e) Z. Li, J. D. Xiao and H. L. Jiang, *ACS Catal.*, 2016, 6, 5359–5365.
- 8 (a) K. G. M. Laurier, F. Vermoortele, R. Ameloot, D. E. De Vos, J. Hofkens and M. B. J. Roeflaers, *J. Am. Chem. Soc.*, 2013, 135, 14488–14493; (b) C. Wang, J. Li, X. Lv, Y. Zhang and G. Guo, *Energy Environ. Sci.*, 2014, 7, 2831–2867; (c) E. M. Dias and C. Petit, *J. Mater. Chem. A*, 2015, 3, 22484–22506; (d) C. C. Wang, X. D. Du, J. Li, X. X. Guo, P. Wang and J. Zhang, *Appl. Catal., B*, 2016, 193, 198–216.
- 9 (a) X. Y. Deng, Z. H. Li and H. García, *Chem. – Eur. J.*, 2017, 23, 11189–11209; (b) X. Yu, L. Wang and S. M. Cohen, *CrystEngComm*, 2017, 19, 4126–4136.
- 10 (a) Y. Lin, C. Kong, Q. Zhang and L. Chen, *Adv. Energy Mater.*, 2017, 7(4), 1601296; (b) E. S. Sanz-Perez, C. R. Murdock, S. A. Didas and C. W. Jones, *Chem. Rev.*, 2016, 116, 11840–11876; (c) J. Liu, P. K. Thallapally, B. P. McGrail, D. R. Brown and J. Liu, *Chem. Soc. Rev.*, 2012, 41, 2308–2322; (d) Y. S. Bae and R. Q. Snurr, *Angew. Chem., Int. Ed.*, 2011, 50, 11586–11596.
- 11 (a) J. W. Maina, C. P. Gonzalo, L. Kong, J. Schütz, M. Hille and L. F. Dumée, *Mater. Horiz.*, 2017, 4, 345–361; (b) H. He, J. A. Perman, G. Zhu and S. Ma, *Small*, 2016, 12, 6309–6324.
- 12 (a) C. Wang, J. Li, X. Lv, Y. Zhang and G. Guo, *Energy Environ. Sci.*, 2014, 7, 2831–2867; (b) E. M. Dias and C. Petit, *J. Mater. Chem. A*, 2015, 3, 22484–22506; (c) C. C. Wang, X. D. Du, J. Li, X. X. Guo, P. Wang and J. Zhang, *Appl. Catal., B*, 2016, 193, 198–216; (d) J. L. Wang, C. Wang and W. Lin, *ACS Catal.*, 2012, 2, 2630–2640; (e) L. Zeng, X. Y. Guo, C. He and C. Y. Duan, *ACS Catal.*, 2016, 6, 7935–7946; (f) A. Dhakshinamoorthy, A. M. Asiri and H. García, *Angew. Chem., Int. Ed.*, 2016, 55, 5414–5445; (g) S. L. Li and Q. Xu, *Energy Environ. Sci.*, 2013, 6, 1656–1683; (h) S. Wang and X. Wang, *Small*, 2015, 11, 3097–3112; (i) M. A. Nasalevich, M. van der Veen, F. Kapteijn and J. Gascon, *CrystEngComm*, 2014, 16, 4919–4926; (j) L. Shen, R. Liang and L. Wu, *Chin. J. Catal.*, 2015, 36, 2071–2088; (k) H. B. Zhang, G. G. Liu, L. Shi, H. M. Liu, T. Wang and J. H. Ye, *Nano Energy*, 2016, 22, 149–168; (l) Y. Hiriuchi, T. Toyao, M. Takeuchi, M. Matsuoka and M. Anpo, *Phys. Chem. Chem. Phys.*, 2013, 15, 13243–13253.
- 13 (a) A. M. Appel, J. E. Bercaw, A. B. Bocarsly, H. Dobbek, D. L. DuBois, M. Dupuis, J. G. Ferry, E. Fujita, R. Hille, P. J. A. Kenis, C. A. Kerfeld, R. H. Morris, C. H. F. Peden, A. R. Portis, S. W. Ragsdale, T. B. Rauchfuss, J. N. H. Reek, L. C. Seefeldt, R. K. Thauer and G. L. Waldrop, *Chem. Rev.*, 2013, 113, 6621–6658; (b) M. Cokoja, C. Bruckmeier, B. Rieger, W. A. Herrmann and F. E. Kuehn, *Angew. Chem., Int. Ed.*, 2011, 50, 8510–8537; (c) M. Cokoja, C. Bruckmeier, B. Rieger, W. A. Herrmann and F. E. Kühn, *Angew. Chem.*, 2011, 123, 8662–8690; (d) E. Fujita, *Chem. Rev.*, 1999, 185–186, 373–384; (e) D. S. Laitar, P. Muller and J. P. Sadighi, *J. Am. Chem. Soc.*, 2005, 127, 17196–17197; (f) A. J. Morris, G. J. Meyer and E. Fujita, *Acc. Chem. Res.*, 2009, 42, 1983–1994; (g) H. Takeda and O. Ishitani, *Chem. Rev.*,

- 2010, **254**, 346–354; (h) C. D. Windle and R. N. Perutz, *Chem. Rev.*, 2012, **256**, 2562–2570.
- 14 L. Duan, F. Bozoglian, S. Mandal, B. Stewart, T. Privalov, A. Llobet and L. Sun, *Nat. Chem.*, 2012, **4**, 418–423.
- 15 (a) S. M. Cohen, *Chem. Rev.*, 2012, **112**, 970; (b) Z. Wang and S. M. Cohen, *Chem. Soc. Rev.*, 2009, **38**, 1315–1329.
- 16 C. Wang, Z. G. Xie, K. E. deKrafft and W. B. Lin, *J. Am. Chem. Soc.*, 2011, **133**, 13445–13454.
- 17 U. J. Ryu, S. J. Kim, H. K. Lim, H. J. Kim, K. M. Choi and J. K. Kang, *Sci. Rep.*, 2017, **7**, 612.
- 18 K. M. Choi, D. Kim, B. Rungtaweevoranit, C. A. Trickett, J. T. D. Barmanbek, A. S. Alshammari, P. D. Yang and O. M. Yaghi, *J. Am. Chem. Soc.*, 2017, **139**, 356–362.
- 19 M. B. Chambers, X. Wang, N. Elgrishi, C. H. Hendon, A. Walsh, J. Bonnefoy, J. Canivet, E. A. Quadrelli, D. Farrusseng, C. M. Draznieks and M. Fontecave, *ChemSusChem*, 2015, **8**(4), 603–608.
- 20 T. Kajiwara, M. Fujii, M. Tsujimoto, K. Kobayashi, M. Higuchi, K. Tanaka and S. Kitagawa, *Angew. Chem.*, 2016, **128**, 2697–2700.
- 21 D. Sun, Y. Gao, J. Fu, X. Zeng, Z. Chen and Z. Li, *Chem. Commun.*, 2015, **51**, 2645–2648.
- 22 H. Fei, M. D. Sampson, Y. Lee, C. P. Kubiak and S. M. Cohen, *Inorg. Chem.*, 2015, **54**, 6821–6828.
- 23 Y. Lee, S. Kim, H. Fei, J. K. Kang and S. M. Cohen, *Chem. Commun.*, 2015, **51**, 16549–16552.
- 24 H. Q. Xu, J. H. Hu, D. K. Wang, Z. H. Li, Q. Zhang, Y. Luo, S. H. Yu and H. L. Jiang, *J. Am. Chem. Soc.*, 2015, **137**, 13440–13443.
- 25 Y. Y. Liu, Y. M. Yang, Q. L. Sun, Z. Y. Wang, B. B. Huang, Y. Dai, X. Y. Qin and X. Y. Zhang, *ACS Appl. Mater. Interfaces*, 2013, **5**, 7654–7658.
- 26 H. B. Zhang, J. Wei, J. C. Dong, G. G. Liu, L. Shi, P. F. An, G. X. Zhao, J. T. Kong, X. J. Wang, X. G. Meng, J. Zhang and J. H. Ye, *Angew. Chem., Int. Ed.*, 2016, **55**, 14310–14314.
- 27 L. Li, S. Q. Zhang, L. J. Xu, J. Y. Wang, L. X. Shi, Z. N. Chen, M. C. Hong and J. H. Luo, *Chem. Sci.*, 2014, **5**, 3808–3813.
- 28 R. Y. Huang, Y. Peng, C. Wang, Z. Shi and W. B. Lin, *Eur. J. Inorg. Chem.*, 2016, **2016**(27), 4358–4362.
- 29 S. Q. Zhang, L. N. Li, S. G. Zhao, Z. H. Sun and J. H. Luo, *Inorg. Chem.*, 2015, **54**, 8375–8379.
- 30 S. Zhang, L. Li, S. Zhao, Z. Sun, M. Hong and J. Luo, *J. Mater. Chem. A*, 2015, **3**, 15764–15768.
- 31 D. Sun, Y. Fu, W. Liu, L. Ye, D. Wang, L. Yang, X. Fu and Z. Li, *Chem. – Eur. J.*, 2013, **19**, 14279–14285.
- 32 D. Sun, W. Liu, M. Qiu, Y. Zhang and Z. Li, *Chem. Commun.*, 2015, **51**, 2056–2059.
- 33 A. S. Portillo, H. G. Baldoví, M. T. G. Fernandez, S. Navalón, P. Atienzar, B. Ferrer, M. Alvaro, H. Garcia and Z. Li, *J. Phys. Chem. C*, 2017, **121**, 7015–7024.
- 34 Y. Lee, S. Kim, J. K. Kang and S. M. Cohen, *Chem. Commun.*, 2015, **51**, 5735–5738.
- 35 D. Sun, W. Liu, Y. Fu, Z. Fang, F. Sun, X. Fu, Y. Zhang and Z. Li, *Chem. – Eur. J.*, 2014, **20**, 4780–4788.
- 36 D. S. Chen, H. Z. Xing, C. G. Wang and Z. M. Su, *J. Mater. Chem. A*, 2016, **4**, 2657–2662.
- 37 S. Wang, W. Yao, J. Lin, Z. Ding and X. Wang, *Angew. Chem., Int. Ed.*, 2014, **53**, 1034–1038.
- 38 S. Wang, J. L. Lin and X. Wang, *Phys. Chem. Chem. Phys.*, 2014, **16**, 14656–14660.
- 39 S. Wang and X. Wang, *Appl. Catal., B*, 2015, **162**, 494–500.
- 40 R. Li, J. Hu, M. Deng, H. Wang, X. Wang, Y. Hu, H.-L. Jiang, J. Jiang, Q. Zhang, Y. Xie and Y. Xiong, *Adv. Mater.*, 2014, **26**, 4783–4788.
- 41 X. He, Z. R. Gan, S. Fisenko, D. W. Wang, H. M. El-Kaderi and W. N. Wang, *ACS Appl. Mater. Interfaces*, 2017, **9**, 9688–9698.
- 42 M. T. Wang, D. K. Wang and Z. H. Li, *Appl. Catal., B*, 2016, **183**, 47–52.
- 43 Q. Liu, Z. X. Low, L. Li, A. Razmjou, K. Wang, J. Yao and H. Wang, *J. Mater. Chem. A*, 2013, **1**, 11563.
- 44 A. Crake, K. C. Christoforidis, A. Kafizas, S. Zafeiratos and C. Petit, *Appl. Catal., B*, 2017, **210**, 131–140.
- 45 Y. Su, Z. Zhang, H. Liu and Y. Wang, *Appl. Catal., B*, 2017, **200**, 448–457.